

Phase-field approach to evolution and interaction of twins in single crystal magnesium

Benhour Amirian^{1*}, Hossein Jafarzadeh², Bilen Emek Abali^{3*}, Alessandro Reali² and James David Hogan¹

^{1*}Department of Mechanical Engineering, University of Alberta, Edmonton, T6G 2R3, AB, Canada.

²Department of Civil Engineering and Architecture, University of Pavia, I-27100, Pavia, Italy.

³Department of Materials Science and Engineering, Uppsala University, 751 21, Uppsala, Sweden.

*Corresponding author(s). E-mail(s): benhour@ualberta.ca; bilenemek@abali.org;

Contributing authors: hossein.jafarzadeh@unipv.it; alereali@unipv.it; jdhogan@ualberta.ca;

Abstract

Crack initiation and propagation as well as abrupt occurrence of twinning are challenging fracture problems where the transient phase-field approach is proven to be useful. Early-stage twinning growth and interactions are in focus herein for a magnesium single crystal at the nanometer length-scale. We demonstrate herein a basic methodology in order to determine the mobility parameter that steers the kinetics of phase-field propagation. The concept is to use already existing molecular dynamics simulations and analytical solutions in order to set the mobility parameter correctly. In this way, we exercise the model for gaining new insights into growth of twin morphologies, temporally-evolving spatial distribution of the shear stress field in the vicinity of the nanotwin, multi-twin, and twin-defect interactions. Overall, this research addresses gaps in our fundamental understanding of twin growth, while providing motivation for future discoveries in twin evolution and their effect on next-generation material performance.

001
002
003
004
005
006
007
008
009
010
011
012
013
014
015
016
017
018
019
020
021
022
023
024
025
026
027
028
029
030
031
032
033
034
035
036
037
038
039
040
041
042
043
044
045
046

047 **Keywords:** Phase-field model; Single crystal magnesium; Twinning
048 interactions; Monolithic scheme

049
050
051

052 1 Introduction

053

054 Developing next-generation materials with controlled twinning behaviors offers
055 promising opportunities for improved mechanical properties [1, 2] and perfor-
056 mance in engineering applications (e.g., gas turbine engines [3] and lightweight
057 automotive structures [4]). Among materials that exhibit twinning [5–8], mag-
058 nesium [9–12] is an example of a light-weight metal where slip and twinning, as
059 the two main crystallographic mechanisms, play a decisive role in its mechan-
060 ical response; however, twinning is favorable on pyramidal $\{10\bar{1}2\}$ $\langle 10\bar{1}1 \rangle$
061 systems at room temperature [13]. In magnesium, single twinning occurs
062 through contraction [14] and extension strains [15] along the c -axis [16]. Recent
063 twinning studies have focused on observations of asymmetric twin growth due
064 to heterogeneous grain deformation in the vicinity of the twin [17, 18]. We
065 understand that interaction of twin boundaries with other defects (i.e., voids
066 and self-interstitials) increases the likelihood for void nucleation, cracking, and
067 premature failure, leading to degradation of material performance and reduc-
068 tion of material lifetime [19, 20]. Recent efforts have also been made to model
069 the twin local stress accurately by means of neighboring grains to accommodate
070 the transformation [21]. In engineering applications, there is a broad interest
071 in incorporating magnesium in high strain-rate applications (e.g., aerospace
072 [22]), where twin growth and evolution limits the mechanical performance [23].
073 However, knowledge gaps in understanding twin growth [24], thickening [25],
074 and interactions [26] need to be addressed before the adoption of magnesium-
075 based alloys into these applications; these are studied herein for a single crystal
076 Mg material system.

077 Ample experimental measurements exist on time-resolved twin evolution
078 in magnesium [27]. In situ data is limited effected by the limitations in avail-
079 able diagnostics to capture growth and evolution behaviors at sufficient length
080 and time scales [28]. To this end, atomistic simulations have been widely
081 adopted to probe effects such as atomic shuffling mechanisms for propagation
082 of twins in magnesium [29], disconnections and other defects associated with
083 the twin interface [30], and reaction of lattice dislocations with twin bound-
084 aries [31]. While new understandings have been gained to accurately model
085 plastic deformation and fracture in magnesium [32, 33], atomistic simulations
086 are limited in their ability to simulate twinning behaviors at relevant length
087 and time scales needed for practical implementations in engineering appli-
088 cations. Challenges also exist in molecular dynamic approaches in applying
089 characterization algorithms (e.g., centrosymmetry parameter [34] and bond
090 angle analysis [35]) to interpret post-deformation crystal structure defect types
091 (e.g., twinning) [36]. Continuum mechanics modeling utilizing crystal plasticity
092

theory is yet another modeling approach for predicting the twinning and detwinning response in materials with hexagonal close-packed crystal structures [37–39]. However, crystal plasticity modeling has difficulties to capture the twinning process correctly due to treating the twinning deformation as a unidirectional shear deformation mode [40]. Additionally, the conventional crystal plasticity model is unable to investigate the effect of twin microstructure on the mechanical behavior of magnesium at the nanometer scale [41]. Overcoming such limitations, we model herein the twinning process by a phase-field approach where the mobility parameter is determined by an inverse analysis. Such a computational implementation allows us to unravel time-evolved twinning behavior in magnesium.

For the morphological evolution of twins, the mesoscale phase-field model [42–47] has been extensively used to study the nucleation [48], growth [49], and propagation of twinning [50]. Most recent computational approaches to phase field equations for studying deformation twinning in magnesium at the microscale were based on the Fourier spectral method [50–52]. However, such an approach is applicable to cases involving periodic boundary conditions and for morphologies and microstructures dominated by long-range elastic interactions [53]. Also, spectral method is mostly used for solving linear problems [54]. In [52, 55, 56], the proposed phase-field simulations for deformation twinning and dislocation induced plasticity in hexagonal closed-pack materials were formulated on small strain theory; still, the twin evolution is usually accompanied by large interface orientation and large shear deformations [57] even under small strains [58]. Thus, coupling between twin evolution and fracture is of importance to achieve high accuracy in the numerical solution. In terms of validating the phase-field results of transmission mechanisms of deformation twins, atomistic simulations (e.g., molecular dynamics simulations [50, 55] and density functional theory [52]) and experimental results [51, 59] are the most widely used. Some drawbacks to these validations exist such as

- discrepancies of the peak stress value from the simulation and experimental data [51],
- qualitative comparison of distribution of order parameter using the isotropic gradient energy parameter [52, 55, 56],
- adopting empirically determined large non-physical values for the phase-field parameters (e.g., twin-twin interfacial energy, initial twin nucleus, and energy barrier heights between the matrix and the twinning [50, 51]), and
- validating at the different length-scales [50, 60].

Hence, the application of their model is somehow limited for studying the deformation mechanisms of Mg. The development of nanoscale phase-field models is therefore required and all the mentioned shortcomings are addressed in this work.

Building on these past works, this current article utilizes a monolithically-solved finite element method for solving an advanced physics-based phase-field approach to study the nanoscale growth of existing twins in anisotropic single

139 crystal magnesium. We follow [61] for modeling the twinning interface prop-
140 agation kinetics, which is important for the realistic description of twinning
141 deformation. The model sheds light on the growth and evolving of twinning
142 embryo.

143 A finite size sample with a hole is considered for studying the interactions
144 of twin with defects, without the need of periodic boundaries. we implement
145 nonlinear elasticity coupled to Ginzburg–Landau equations for order paramete-
146 rs. By using a highly nonlinear phase-field approach, we model anisotropic
147 surface energy allowing to simulate large deformation of defect-free volumes at
148 the nanoscale. Motivated by the literature [62–66], we use a mobility param-
149 eter and devote the work for determining this value for a specific material,
150 namely single crystal Mg. The time evolution of the twin order parameter is
151 directly proportional to the resolved shear stress. This outcome is useful for
152 modeling deformation twinning since the propagation speed of twin boundaries
153 is rather difficult to measure experimentally, and could even be supersonic if
154 the driving stress is sufficiently large [67].

155 We verify the proposed implementation of the time-resolved continuum-
156 based model for magnesium by the static phase-field model [68] and molecular
157 dynamics (MD) simulations [69] (Fig. 1). By choosing the same length-scale
158 for the phase-field model and MD simulations, we assure the compatibility of
159 MD results with our implementation, which is often left aside in the literature
160 [51, 56, 60]. It is also worth stating that all MD simulations use extremely high
161 deformation rates, making it difficult to understand whether a phenomenon
162 results from the rate sensitivity of the material or is a numerical artifact [?
163 ?]. However, various strategies can be used to bridge the gap between the
164 atomic scale and continuum frameworks, such as large-scale MD calculations
165 [?], coarse-graining [?], and ultra-high strain-rate tests [?]. Twin propagation
166 speed is explored (Fig. 2) and compared with MD results [69] and analytical
167 solutions [70]. In this way, we demonstrate a simple yet effective approach how
168 to determine the mobility parameter. Moreover, insights in growth rates are
169 of interest given the limited available data [27] and studying these behaviors
170 is vital in high-rate applications of magnesium [71]. Our presented results are
171 then validated in terms of twin area fraction and global shear stress (Fig. 3),
172 and the role of twin-twin and twin-defect interactions is explored (Fig. 4).
173 Through these approaches, the research offers broad potential in materials
174 design, and motivates promising directions in experimental and computational
175 materials science.

176

177 2 Governing equations

178

179 We use standard continuum mechanics notation, where Latin indices refer
180 to spatial coordinates. We understand Einstein’s summation convention over
181 repeated indices. All tensors are expressed in Cartesian coordinates. The super-
182 scripts E and IE stand for elastic (recoverable) and inelastic (irreversible)

183

184

deformations, respectively. For the description of the twin, an order (phase-field) parameter, η , is introduced, where $\eta = 0$ denotes the parent crystal and $\eta = 1$ means the twin. This order parameter as well as displacement, \mathbf{u} , are the primitive variables in space and time that we are searching for. The deformation gradient reads

$$F_{ij} = u_{i,j} + \delta_{ij} , \tag{1}$$

where comma denotes a derivative in space. We use a material frame, where the derivative is taken in the reference configuration that is chosen to be the initial placement of the continuum body. Kronecker delta, δ , is the identity. The deformation gradient, \mathbf{F} , in a large-displacement formulation, is decomposed into elastic and inelastic parts,

$$F_{ij} = F_{ik}^E F_{kj}^{IE} , \tag{2}$$

where for (inelastic) twinning [72], we use

$$F_{ij}^{IE} = \delta_{ij} + \phi(\eta)\gamma_0 s_i m_j . \tag{3}$$

The interpolation function, $\phi(\eta) = \eta^2(3 - 2\eta)$, causes a steep change between twin and parent crystal [73] as necessary in phase-field approaches, γ_0 is the magnitude of maximum twinning shear, and \mathbf{s} and \mathbf{m} are the unit vectors along the twinning direction and normal to the twinning plane, respectively. By following [74], we decompose the Helmholtz free energy per mass into mechanical and interfacial parts,

$$\psi(\mathbf{F}, \eta, \nabla\eta) = \psi^M(\mathbf{F}, \eta) + \psi^\nabla(\eta, \nabla\eta) , \tag{4}$$

where kinetics of interface is controlled by twin order parameter and its first-gradient by the latter. As usual, for the mechanical deformation energy density (per volume), we may use the St. Venant model:

$$\rho_0 \psi^M = \frac{1}{2} E_{ij} C_{ijkl} E_{kl} , \tag{5}$$

or the neo-Hookean model:

$$\rho_0 \psi^M = \frac{\mu}{2} (I_C - 3) - \mu \ln J + \frac{\lambda}{2} (\ln J)^2 . \tag{6}$$

For nonlinear isotropic elasticity, the neo-Hookean model defined in Eq. (6) is used. We use right Cauchy–Green deformation tensor, $C_{ij}^E = F_{ki}^E F_{kj}^E$, and its invariants, $I_C = C_{ii}^E$, $J = \det(\mathbf{C}^E)$. The Green–Lagrange strain measure, $\mathbf{E} = \frac{1}{2}(\mathbf{C}^E - \delta)$, accommodates geometric nonlinearity necessary for some applications herein. Lamé parameters, λ , μ , or the stiffness tensor of

185
186
187
188
189
190
191
192
193
194
195
196
197
198
199
200
201
202
203
204
205
206
207
208
209
210
211
212
213
214
215
216
217
218
219
220
221
222
223
224
225
226
227
228
229
230

rank four, C_{ijkl} , are given as material coefficients. The elastic constants are the Voigt-averaged shear and bulk modulus [75], which are listed in Table 1. For anisotropic elasticity, the elastic coefficients are interpolated between the untwinned C_{ijkl}^P and twinned C_{ijkl}^T domains using the interpolation function,

$$C_{ijkl} = C_{ijkl}^P + (C_{ijkl}^T - C_{ijkl}^P)\phi(\eta) . \quad (7)$$

The same interpolation function is used as in the definition of inelastic part of the deformation gradient. For the twin phase, $\eta = 1$, we have the stiffness tensor as a rotation of crystal lattice from the parent phase, $\eta = 0$, as follows:

$$C_{ijkl}^T = Q_{im}Q_{jn}Q_{ko}Q_{lp}C_{mnop}^P, \quad (8)$$

where \mathbf{Q} is the reorientation matrix associated with twinning, for a centrosymmetric structure [76], it becomes

$$Q_{ij} = \begin{cases} 2m_i m_j - \delta_{ij} & \text{type I twins,} \\ 2s_i s_j - \delta_{ij} & \text{type II twins.} \end{cases} \quad (9)$$

In the case of a steady-state deformation by neglecting inertial terms, governing equations for displacement read

$$P_{ji,j} = 0 , \quad P_{ji} = \frac{\partial \rho_0 \psi}{\partial F_{ij}} = \frac{\partial \rho_0 \psi^M}{\partial F_{ij}} = \frac{\partial \rho_0 \psi^M}{\partial E_{kl}} \frac{\partial E_{kl}}{\partial F_{ij}} = \frac{\partial \rho_0 \psi^M}{\partial E_{kl}} F_{il}^E (F^{IE})_{jk}^{-1} . \quad (10)$$

The Ginzburg–Landau equation is acquired by a thermodynamically-consistent derivation, as follows:

$$\dot{\eta} = -\mathcal{L} \left(\frac{\partial \rho_0 \psi^M}{\partial \eta} + \frac{\partial \rho_0 \psi^\nabla}{\partial \eta} - \left(\frac{\partial \rho_0 \psi^\nabla}{\partial \eta_{,i}} \right)_{,i} \right) , \quad (11)$$

where the mobility parameter, \mathcal{L} , is generally not known and challenging to obtain experimentally. The outcome of this work is the methodology how to set its numerical value.

The first term is formulated by using the product rule

$$\frac{\partial \rho_0 \psi^M}{\partial \eta} = \frac{\partial \rho_0 \psi^M}{\partial F_{ij}} \frac{\partial F_{ij}}{\partial \eta} = P_{ji} \frac{\partial F_{ik}^E F_{kj}^{IE}}{\partial \eta} = P_{ji} F_{ik}^E \phi'(\eta) \gamma_0 s_k m_j , \quad (12)$$

where $\phi'(\eta) = 6\eta(1 - \eta)$. For the interfacial energy, ψ^∇ , we use a standard double-well potential as in [77, 78] such that the energy density reads

$$\rho_0 \psi^\nabla(\eta) = A\eta^2(1 - \eta)^2 + \kappa_{ij}\eta_{,i}\eta_{,j} , \quad (13)$$

where $A = 12\frac{\Gamma}{l}$ characterizes the energy barrier between two stable phases (minima), related to the twin boundary surface energy, Γ , and the twin boundary thickness, l ; $\kappa_{ij} = \kappa_0\delta_{ij}$ with κ_0 being the gradient energy parameter, given as [68], $\kappa_0 = \frac{3}{4}\Gamma l$. By inserting the energy definitions into the Ginzburg–Landau, we obtain the governing equation for twin order parameter,

$$\dot{\eta} = -\mathcal{L}\left(P_{ji}F_{ik}^E\phi'(\eta)\gamma_0s_km_j + 2A\eta(1 - 3\eta + 2\eta^2) - 2\kappa_0\eta_{,ii}\right) \quad (14)$$

By solving Eqs. (10), (14), we obtain \mathbf{u} and η fields.

3 Computational implementation

The presented numerical simulations employ a monolithic strategy in order to solve Eqs. (10), (14). Because of their inherent coupling, a monolithic solution method is preferable for capturing all effects accurately, especially in extreme loading conditions. Mostly, a staggered scheme is implemented partly to increase efficiency yet also effected by numerical difficulties in implementing as monolithic strategy. Herein we use the interface energy as described above, which helps to circumvent any numerical convergence errors in the implementation. In a monolithic scheme, for each time step, displacements and order parameter are solved at once. Therefore, for the space discretization, we use an adequate mixed space formulation in the implementation. Specifically, we use \mathbf{u} and η as approximated functions spanned over a triangulation with a compact support. This well-known finite element method (FEM) ensures a monotonic convergence for the implementation. We skip a notational distinction between the analytical functions and their approximations since they never show up together.

The computational domain, Ω , is the continuum body's image in the physical space. The domain, Ω , and its closure as a Lipschitz boundary, $\partial\Omega$, form a continuous domain without singularities. Therefore, all form functions are continuous as well. Triangulated domain in finite number of nodes is representing the approximated unknown functions, \mathbf{u} and η , with the interpolation between the nodes by the form functions, as follows:

$$\mathcal{V} = \left\{ \{ \mathbf{u}, \eta \} \in [\mathcal{H}^n(\Omega)]^{\text{DOF}} : \{ \mathbf{u}, \eta \} = \text{given } \forall \mathbf{x} \in \partial\Omega_D \right\}. \quad (15)$$

The Hilbertian Sobolev space, \mathcal{H}^n , is of polynomial order, n , hence, we use standard Lagrange elements in the FEM [79]. On each node, we have $2 + 1 = 3$ degrees of freedom (DOFs) in two-dimensional and $3 + 1 = 4$ (DOFs) in three-dimensional spaces. As known as Galerkin approach, the test functions, $\delta\mathbf{u}$ and $\delta\eta$, are approximated by the same mixed space. They vanish on Dirichlet boundaries, $\partial\Omega_D$, where the solution, \mathbf{u} or η , is given. For other boundaries, we use Neumann boundary condition, for displacement, \mathbf{u} , it denotes the given

323 traction vector, $\hat{\mathbf{t}}$, and for twin order parameter, η , we implement zero Neu-
 324 mann boundaries meaning that the twin phase fails to leave the boundary
 325 across boundaries. The latter is justified easily since the twin or parent phase is
 326 neither convective nor conductive. The twin growth is inhibited by the displace-
 327 ment boundary conditions. The twin order parameter gradient also vanishes
 328 at the boundaries due to the Neumann boundary condition.

329 For time discretization, we use constant time steps in order to be able to
 330 determine an adequate time step by a convergence analysis. Given the data at a
 331 time instant, t^n , we solve \mathbf{u} and η by a standard variational formulation leading
 332 to a weak form. The time derivative of order parameter is discretized using a
 333 so-called θ -scheme, for an arbitrary field, $y^n = y(t^n)$ and $y^{n-1} = y(t^{n-1})$, we
 334 use

$$335 \quad y^{n-\theta} = (1 - \theta)y^{n-1} + \theta y^n . \quad (16)$$

336 This scheme requires the computed solution from the last time step, y^{n-1} , by
 337 evaluating the functions within the time step leading to a higher accuracy in
 338 the discretization [80]. For $\theta = 0$, this method is the first-order accurate explicit
 339 Euler method. For $\theta = 1$, it becomes the first-order accurate implicit Euler
 340 method. For $\theta = 0.5$, we obtain the second-order accurate Crank–Nicolson
 341 method. We use the time discretization in Eq. (14) for one finite element Ω^e ,
 342 as follows:

$$343 \quad \int_{\Omega^e} \left(\frac{\eta^n - \eta^{n-1}}{\Delta t} + \mathcal{L} \left(P_{ji} F_{ik}^E \phi'(\eta^{n-\theta}) \gamma_0 s_k m_j + 2A\eta^{n-\theta} (1 - 3\eta^{n-\theta}) \right. \right. \\ 344 \quad \left. \left. + 2(\eta^{n-\theta})^2 - 2\kappa_0 \eta_{,ii}^{n-\theta} \right) \right) \delta\eta \, dV = 0 . \quad (17)$$

350 The test function, $\delta\eta$, may have a lower continuity than the trial function,
 351 η , but we stress that we aim for the Galerkin procedure such that they are
 352 chosen from the same mathematical space. In order to weaken the continuity
 353 condition on η , we integrate by parts terms of second gradient,

$$354 \quad \int_{\Omega^e} \left(\frac{\eta^n - \eta^{n-1}}{\Delta t} \delta\eta + \mathcal{L} P_{ji} F_{ik}^E \phi'(\eta^{n-\theta}) \gamma_0 s_k m_j \delta\eta \right. \\ 355 \quad \left. + \mathcal{L} 2A\eta^{n-\theta} (1 - 3\eta^{n-\theta} + 2(\eta^{n-\theta})^2) \delta\eta + 2\mathcal{L}\kappa_0 \eta_{,i}^{n-\theta} \delta\eta_{,i} \right) dV \quad (18) \\ 356 \quad - \int_{\partial\Omega^e} 2\mathcal{L}\kappa_0 \eta_{,i}^{n-\theta} n_i \, dA = 0 .$$

357
 358
 359
 360
 361
 362
 363
 364 By summing over each element, on each boundary of elements we sum twice
 365 with neighboring elements' surface normal directed oppositely. Therefore, we
 366 obtain a jump condition, which we enforce to vanish by setting it zero. In other
 367 words, the weak formulation searches for a continuous $\eta_{,i} n_i$ across element
 368 boundaries resulting a smooth phase change within the finite element. In this

way, a mesh dependency is prevented as long as the element size is adequately small such that the numerical result is converged. On the boundaries of the whole domain, we assume zero Neumann boundaries meaning that η is not leaving the domain across the outer boundary. Hence, we obtain for $\Omega = \bigcup \Omega^e$, the following weak form:

$$\begin{aligned} \text{Form}_\eta = \int_\Omega & \left(\frac{\eta^n - \eta^{n-1}}{\Delta t} \delta\eta + \mathcal{L} P_{ji} F_{ik}^E \phi'(\eta^{n-\theta}) \gamma_0 s_k m_j \delta\eta \right. \\ & \left. + \mathcal{L} 2A \eta^{n-\theta} \left(1 - 3\eta^{n-\theta} + 2(\eta^{n-\theta})^2 \right) \delta\eta + 2\mathcal{L} \kappa_0 \eta_{,i}^{n-\theta} \delta\eta_{,i} \right) dV . \end{aligned} \quad (19)$$

Analogously, from Eq. (10), we obtain the weak form for displacement, where the traction $t_i = n_j P_{ji}$ is enforced to be continuous across the element. This so-called Newton's second lemma is a basic assumption for regular domains (no singularities). On outer boundaries, for Dirichlet boundaries, where displacement is given, the test function vanishes and we allow for Neumann boundaries that traction vector, $\hat{\mathbf{t}}$ in Pa, is given. The weak form for displacements, \mathbf{u} , reads

$$\text{Form}_\mathbf{u} = - \int_\Omega P_{ji} \delta u_{i,j} dV + \int_{\partial\Omega_N} \hat{t}_i \delta u_i dA . \quad (20)$$

The objective is to solve both fields as unknowns, $\mathbf{p} = \{\mathbf{u}, \eta\}$, at once by satisfying

$$\text{Form}_\eta + \text{Form}_\mathbf{u} = 0 . \quad (21)$$

The weak form is nonlinear. We use a standard Newton–Raphson linearization method, where the weak form is used to get a Jacobian by a derivative with respect to unknowns, \mathbf{p} . High-level tools are exploited to generate computer code automatically by performing a symbolic differentiation for this linearization. In this manner, use of different stored energy models is indeed possible without major changes in the implementation. We use software packages from the FEniCS Project [81, 82]. The time stepping parameters are chosen such that the momentum balance scheme is second-order accurate and stable. Quadratic and linear Lagrange functions are used for the finite element approximation of the displacement and the twin order parameter, respectively. The conjugate gradient method with a Jacobi preconditioner from PETSc packages [83] has been employed for solving the nonlinear equations. The simulation has been performed by a computing node using Intel Xeon E7-4850, in total 64 cores each with the 40 MB cache, equipped with 256 GB Memory in total, running Linux Kernel 5 Ubuntu 20.04.

4 Results and discussion

The material parameters are compiled from different sources and given in Table 1. For anisotropic cases, we use stiffness tensor with the given components and isotropic cases the Lamé constants, λ , μ . The computational domain

415 is a 2-D rectangular shape at nanometer (nm) length-scale. Accordingly, units
416 are chosen to be nanonewton (nN) and picosecond (ps). A mesh of 423 500
417 triangular elements is adopted. Initial conditions are prescribed as zero dis-
418 placement and a given twin/parent phase field, which is described in each
419 example. It is noted that 10 elements are considered at the interface to resolve
420 the sharp variation along the interface width.

421

422 **Table 1** Material properties and model constants for single crystal magnesium compiled
423 from [16, 25, 69, 77, 84]

424

Parameters	Notation	Value
	$C_{11} =$	63.5 GPa
	$C_{12} =$	25.9 GPa
Second order elastic constants	$C_{13} =$	21.7 GPa
	$C_{33} =$	66.5 GPa
	$C_{44} =$	18.4 GPa
Bulk modulus	$K =$	36.9 GPa
Shear modulus	$\mu =$	19.4 GPa
Poisson's ratio	$\nu =$	0.276
Twin boundary surface energy	$\Gamma =$	0.117 J/m ²
Twinning shear for $\langle 10\bar{1}1 \rangle \{ \bar{1}012 \}$	$\gamma_0 =$	0.1295
Regularization length	$l =$	1.0 nm
Transformation barrier	$A =$	1.404 GPa
Gradient energy parameter	$\kappa_0 =$	0.0878 nJ/m
Ginzburg–Landau kinetic factor	$\mathcal{L} =$	4200 (Pa · s) ⁻¹

442

443

444

445 4.1 Validation of the phase-field model and twin order 446 parameter for single crystal magnesium 447

448 We validate our time-resolved phase-field model for single crystal magne-
449 sium using previous static phase-field results [68] and molecular dynamics
450 simulations [69] (Fig. 1). The presence of pronounced mechanical anisotropy,
451 local stress concentrations, and high pressure in nanoscale defect-free magne-
452 sium implies employing anisotropic mechanical properties, anisotropic surface
453 energy, and a large displacement formulation in our simulations. The nucle-
454 ation and evolution of deformation twinning in a magnesium single crystal
455 is simulated using the same initial twin geometry as in [68]. A circular twin
456 embryo of initial radius $r = 3$ nm (corresponding to the analytical sharp
457 interface solution [85]) is embedded into a rectangular domain of dimensions
458 40 nm × 40 nm in plane strain conditions. The $\langle 10\bar{1}1 \rangle$ plane and $\{ \bar{1}012 \}$ direc-
459 tions are considered as the primary twinning system [86]. Consequently, there
460 is no need to assume the dependency of the mobility parameter to the angle

between the direction normal to the interface and a specified direction in crystal as well as temperature, due to the fact that the kinetic coefficients differ by only about 1% in different planes and directions [?]. The validation simulations in Fig. 1 are performed to investigate the twin parameter distribution subject to simple shear with Dirichlet boundary conditions on the order parameter for different cases, including an isotropic (Fig. 1(a, c, d, g, h)) and an anisotropic surface energy (Fig. 1(b, e, f, i, j)) at three different time instants. Within the simulation time of 500 ps, the twin embryo grows until it is repelled by the rigid outer boundaries. For the anisotropic case, the equilibrium shape of the twin embryo is wider in the horizontal direction (parallel to the habit plane) and flatter normal to the habit plane when compared with the isotropic case, which is in good qualitative agreement with the reference phase-field results [68] shown in Fig. 1(m). In addition, the twin interface thickness has a lower value normal to the habit plane for the anisotropic surface energy when compared with the ideal isotropic one. This may be related to the contribution of the core and elastic energies to the total surface energy of the interface [87]. For large deformation simulations (Fig. 1(b, d, f, h, j)), an orientation of the twin evolution is realized due to the difference in the driving force for twinning, which is a factor of $(F^\eta)^{-1}$. Overall, the twin shape predicted by the current time-dependent phase-field approach shows features in good agreement with the molecular dynamics simulation [69] (Fig. 1(k)) and steady-state continuum-based model [68] (Fig. 1(l, m)). Finally, it is worth mentioning that the twin tends to shrink and eventually disappear when the magnitude of the shear loading was lower than $\gamma_0 = 0.07$ or the size of the initial nucleus were lower than 3 nm. This detwinning mechanism has been observed previously in copper [88] and gold nanowires [89], but this is not the focus of the present contribution.

4.2 The determination of the kinetic coefficient, \mathcal{L} , for magnesium using twin tip and twin boundary velocities

The kinetic coefficient or mobility parameter, \mathcal{L} , plays an important role in describing the twin propagation and its dependence on other parameters (e.g., shear stress) during the early stages of twin morphology [90, 91]. Experimental studies lack a quantification of the twin boundary mobility in magnesium since the evolution is too quick for obtaining an adequate measurement. In order to address this, we propose to determine \mathcal{L} for single crystal magnesium by using interface velocity profiles in both twin tip and twin boundary directions by comparing the present time-resolved phase-field results with molecular dynamics simulations [69] (Fig. 2). Here we assume that the molecular dynamics solution represents a reliable experiment and try to find the kinetic coefficient such that we obtain matching results. Considering a single twinning plane and direction as the primary deformation mechanism, an isotropic kinetic coefficient is obtained for predicting the microstructure evolution in two-dimensional single crystal magnesium at room temperature. This assumption is consistent

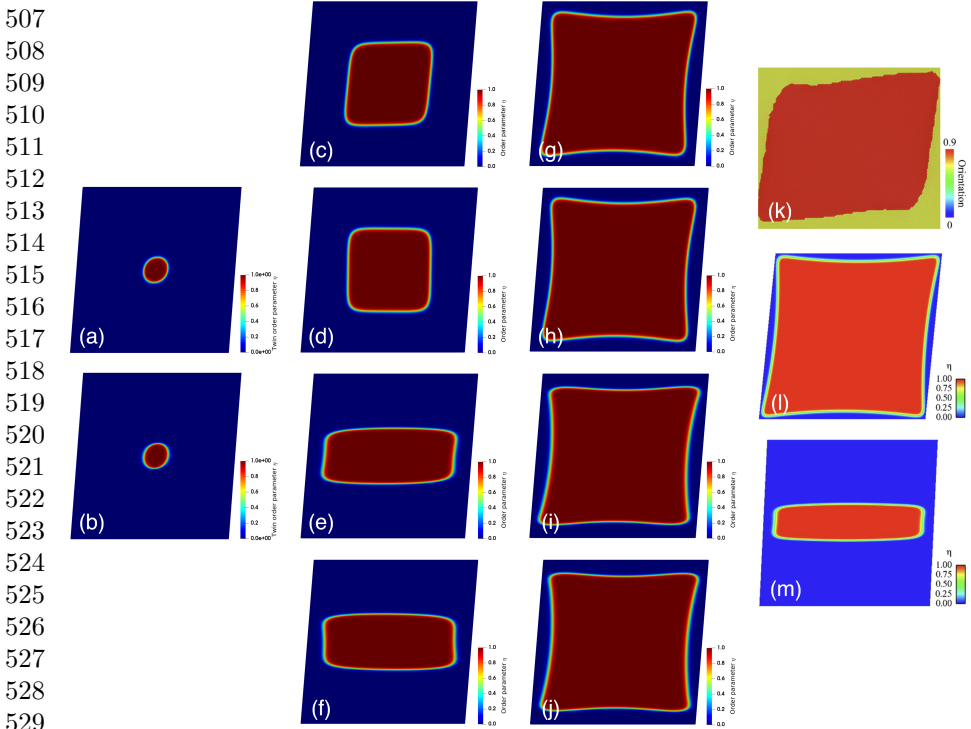


Fig. 1 Distribution of the twin order parameter, η , for an initially circular single twin with radius of 3 nm in a simple-sheared rectangular domain in both small and large deformations considering both isotropic and anisotropic surface energy and elasticity with zero orientation of the habit plane. The initial conditions are chosen to match results published in the literature using a static phase-field approach [68] and molecular dynamics model [69], while the choice of times are selected to show the evolution of the twin growth under noted conditions. (a,b) Twin order parameter for small and large strains with an isotropic surface energy at $t = 1$ ps; (c,d) Twin order parameter for small and large strains and isotropic surface energy at $t = 50$ ps; (e,f) Twin order parameter for small and large strains and anisotropic surface energy at $t = 50$ ps; (g,h) Twin order parameter for small and large strains and isotropic surface energy at $t = 500$ ps; (i,j) Twin order parameter for small and large strains and anisotropic surface energy at $t = 500$ ps; (k) Local orientation of the twinned region obtained from molecular dynamics simulations [69] and used to contrast with (g) and (h); (l,m) Order parameter for both isotropic and anisotropic surface energy under simple shear loading using a phase-field model from the literature [68], to be compared with (e) and (g). (k) and (l,m) are reproduced with permission from [68] and [69], respectively. (For interpretation of the references to color in this figure, the reader is referred to the web version of this article.)

with the other atomistically informed phase-field model [52, 55]. Although, taking into account an anisotropic kinetic coefficient which depends on free energy functional parameters (e.g., temperature or interface orientation) is required to accurately describe the other phase transformation (e.g., liquid-liquid, liquid-vapor, and solid-melt phase transformations) interface kinetics [92]. A rectangular twin embryo with an initial length of 7 nm and width of 4.3 nm inserted at the center of a $77 \text{ nm} \times 55 \text{ nm}$ rectangular domain as in

Fig. 2(a). The domain is under simple-shear, the $(\bar{1}012)$ twinning planes (i.e., the horizontal planes) are referred to as twin boundaries (TB), and the $(10\bar{1}2)$ twinning planes (i.e., the vertical planes) are referred to as twin tips (TT). Applying the shear deformation in the $[10\bar{1}1]$ direction results in the twin interface profiles illustrated in Figs. 2(b) and 2(c) for the twin boundary and twin tip for times noted in the sub-figures, respectively. The twin boundary and twin tip velocities are calculated by tracking the horizontal, Δx , and vertical, Δy , interface displacement of the planes of the twin at $\eta = 0.5$ over time—along the green line in Figs. 2(b) and 2(c). The results indicate that the twin boundary (black color) and twin tip (blue color) velocities are decreasing and constant, respectively, with values of velocity summarized in Fig. 2(d). The constant velocity trend of twin tip mobility may be ascribed to the large back-stress arising at the twin tip [90]. Mapped in red onto Fig. 2(c) is the explicit analytical solution for the stationary Ginzburg–Landau equation given by [70]

$$\eta_{\text{analytical}} = \left(1 + \exp\left(\frac{-x}{w}\right)\right)^{-1}; \quad w = \sqrt{\frac{\kappa_0}{2A}}. \quad (22)$$

The comparison of numerical results with this analytical solution enables the twin interface width (i.e., difference between twin interface position at $\eta = 0.01$ and $\eta = 0.99$) to be calculated. The determination of the twin interface width is important because its size can guide the selection of the element size and spatial mesh refinement in finite element simulations of twinning [78]. Altogether, Fig. 2 provides a good validation for the present time-dependent phase-field approach, and, more importantly, enables the first ever determination of the kinetic energy coefficient, $\mathcal{L} = 4200 \text{ (Pa} \cdot \text{s)}^{-1}$, for single crystal magnesium.

4.3 The time-evolved shear stress in the combined matrix-twin embryo

For a better comprehension of the underlying mechanism, we study the evolution of the twin area fraction and the shear stress, σ_{12} , in the parent and twin phase (Fig. 3). Local stress distribution within a small region in the microstructure is understood as the driving force for the propagation and growth of a twin. These insights may inform about the sequence of events leading to the formation of the visible twins at an early stage in magnesium. In Fig. 3, the same boundary conditions and a constant 7% shear strain are used in the same rectangular twin embryo system depicted in Fig. 2(a). Initially, the length and width of a single rectangular twin embryo at different times are calculated in Fig. 3(a); this will be used to obtain the twin area fraction in Fig. 3(b). In the figure, values are calculated for $\eta = 0.5$ on the interface profile as shown in the insets at $t = 5 \text{ ps}$. Results indicate that the twin growth is larger in the twin tip direction rather than in the twin boundary direction, and this difference decreases at later time instants as the twin approaches the outer boundaries.

Next, the change of the twin area fraction, defined as the ratio of the twinned to the whole simulated area, is shown in Fig. 3(b) under shear loading,

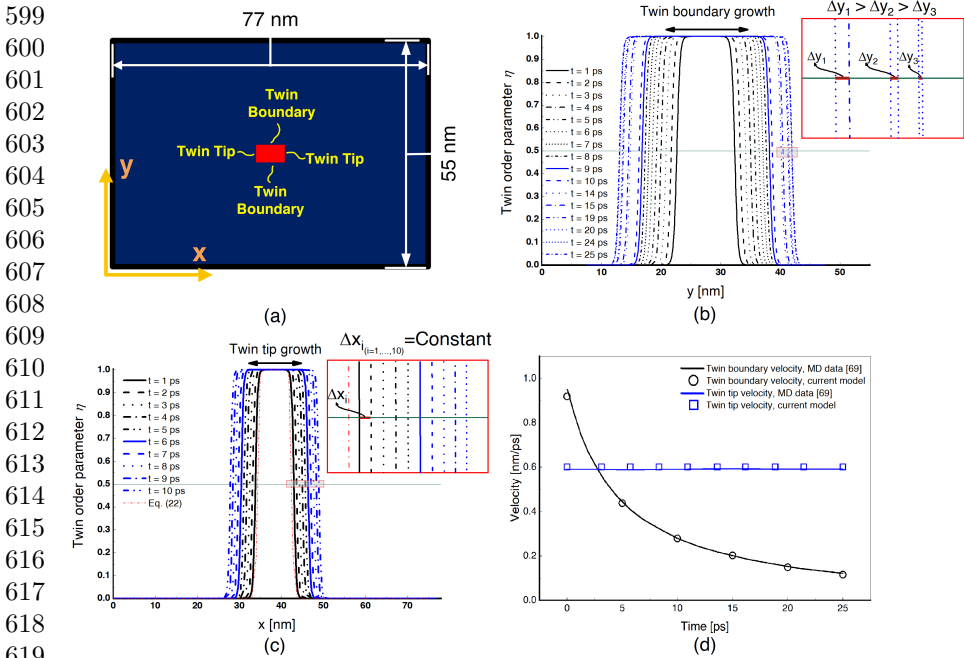


Fig. 2 Evolution of twin growth in a single-crystal pure magnesium. (a) Numerical setup of the rectangular single crystal with an initial rectangular twin with boundaries and tips in material configuration; (b) Time evolution of the twin order parameter as a function of the position y normal to the habit plane. A horizontal line starting from point $\eta = 0.5$ is chosen for measuring the twin boundary interface velocity to show the interface displacement Δy . The inset demonstrates the interface profile at six different time instants to show the time-dependent growth of the twin; (c) Time evolution of the twin order parameter as a function of the position x in the direction of the habit plane. Fewer time instants than shown in (b) are used to demonstrate the constant twin tip interface velocity. Similarly, the point $\eta = 0.5$ is chosen for measuring the tip interface velocity and to show the constant interface displacement Δx . The analytical solution of the explicit Ginzburg–Landau equation, which corresponds to $t = 0$ ps, is shown as the dotted red color; (d) Twin tip and twin boundary velocities as a function of time obtained from (b) and (c), and compared with those from the molecular dynamics simulations [69]. (For interpretation of the references to color in this figure, the reader is referred to the web version of this article.)

and this is compared with molecular dynamics simulations [69]. The insets in Fig. 3(b) show the morphology of the twin at two different times for visualizing how the twins grow. Knowing the twin area fraction evolution is important towards enhancing our understanding of the crystal grain reorientation associated with deformation twinning, where limited data exists because of the special experimental tools needed to access the length and time scales needed to capture such measurements [27]. As seen in Fig. 3(b), the present phase-field model reasonably predicts the evolution of the twin area fraction. Next, the shear stress profile acting parallel to the x -direction is plotted for various times in Fig. 3(c), which is used to demonstrate the redistribution of internal

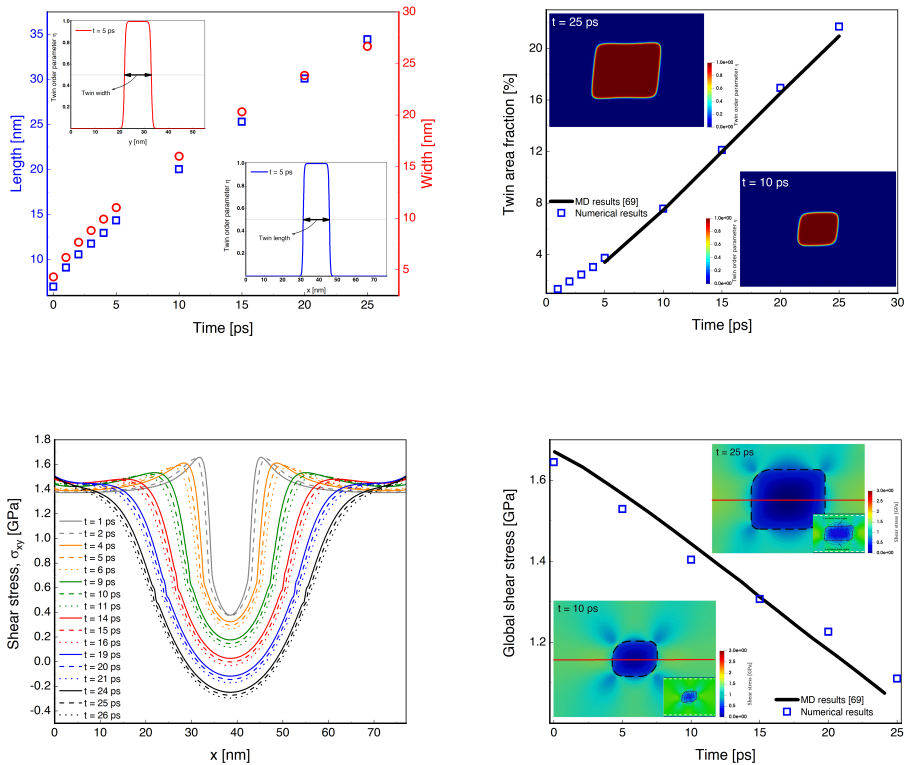


Fig. 3 The time-evolved shear stress acquired from the phase-field model on deformation twinning of single-crystal pure magnesium. (a) Time evolution of the length (blue squares) and width (red circles) of a single rectangular twin embryo that grows at 7% shear strain. The insets show the twin interface profiles at $t = 5$ ps, parallel and orthogonal to the habit plane, by which the twin size is obtained; (b) Growth of the twin area fraction (i.e., the ratio of twinned area to the total area of the numerical geometry) predicted by the proposed phase-field approach (blue squares) and compared with molecular dynamics simulations (black line) [69]. The same numerical geometry setup as [69] was used. The insets show the distribution of the twin order parameter at $t = 10$ ps and $t = 25$ ps to illustrate areal growth; (c) Spatial variation of initial shear stress along the x -axis in single-twinned magnesium at various time instants; (d) Variation of the global shear stress as a function of time. The numerical results (blue squares) are compared with molecular dynamics data (black line) [69]. The insets show the spatial distribution of local shear stress at $t = 10$ ps and $t = 25$ ps along the red mid-line. The boundaries of the twin embryo are denoted by the black dashed line. In the bottom of each inset, the atomic shear stress from snapshots taken at similar times as [69] are given for comparison. (For interpretation of the references to color in this figure, the reader is referred to the web version of this article.)

stresses resulting from twinning [93]. The plateau and decreasing regions indicate the shear stress variation in the parent and twin phases, respectively. By progressing in time, the shear stress decreases as the x -position approaches the center of the simulation geometry, until it reaches its minimum. The magnitude of the shear stress within the twin decreases as a function of time and, eventually, becomes negative for the last time instants of the simulation. This

645
646
647
648
649
650
651
652
653
654
655
656
657
658
659
660
661
662
663
664
665
666
667
668
669
670
671
672
673
674
675
676
677
678
679
680
681
682
683
684
685
686
687
688
689
690

691 phenomenon is consistent with experimental results [17]. At the same time,
692 the profile evolves spatially and temporally.

693 Finally, the global shear stress field is shown in Fig. 3(d), where the field
694 is taken as the average across the red line spanning both the twin and the
695 matrix depicted in the inset. The measurements are important because they
696 can provide insights into the complex load sharing mechanisms that are gener-
697 ated by the parent and the twin phase [94]. The results are also compared with
698 molecular dynamics simulations [69], both qualitatively (the insets at $t = 10$ ps
699 and $t = 25$ ps) and quantitatively. The phase-field results match the molecu-
700 lar dynamics simulations well. The results show that the global shear stress is
701 decreasing as the twin size evolves. Altogether, results from Fig. 3 are impor-
702 tant for determining the activation force required for twin embryo growth that
703 may serve as an input into higher scale models [95].

704

705 4.4 Studying twin interactions toward microstructure 706 tailoring and materials design 707

708 Finally, simulations have been performed to study the effect of twin-twin
709 and twin-defect interactions (Fig. 4). Understanding these interactions is an
710 important step toward developing better predictive models for designing materi-
711 als with tailored properties [96–99] and microstructures [100–103]. Damage
712 in materials is studied by phase-field models [104–108], we use phase-field
713 approach herein for twin interactions. This interactions [109] may result in the
714 formation of twin-twin junctions that may cause strain hardening [110] and
715 crack initiation [111, 112], leading to a strong influence on the overall mater-
716 ial performance. First, the change of area fraction of the middle twin as a
717 function of time for a different number of embryos is illustrated in Fig. 4(a).
718 Only the middle embryo is considered in the analysis in order to better iso-
719 late the interactions and reduce boundary effects. The location of the twins
720 for the three embryo cases is illustrated in the inset. In Fig. 4(a), it is shown
721 that increasing the number of twins leads to a decrease in the twin area frac-
722 tion of the middle embryo as a result of its interaction with the other twins.
723 The difference of the twin area fraction for multi-embryo cases becomes larger
724 at later time instants. This finding is important as it highlights the effects
725 of twin interactions on twin evolution, where experimental measurements are
726 currently very limited [113]. Next, the spatial variation of the order param-
727 eter and the corresponding shear stress at $t = 10$ and $t = 20$ ps are depicted
728 in Fig. 4(b). This result reveals insights into the expansion of the twin domain
729 through the accumulation of large plastic shear strain at the nano-scale [114].

730 The homogeneous growth in the twin area is exemplified in the top left
731 inset in Fig. 4(b), where the twins have not changed in shape until $t = 10$ ps.
732 The corresponding shear stress distribution at $t = 10$ ps is shown in the bottom
733 left inset, where the shear stress inside the twins is negative while it is positive
734 in the matrix. The heterogeneous stress distribution around the twins is due
735 to a sudden change in the stresses within the twin interfaces, associated with
736 the need to accommodate deformation in this region [40]. From the spatial

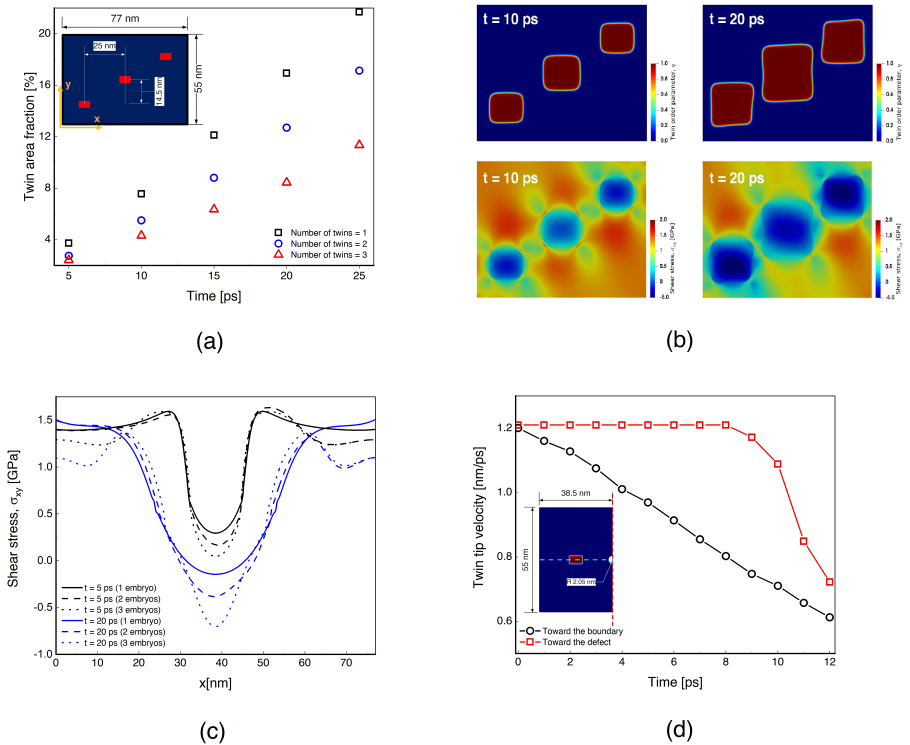


Fig. 4 Exploration of twin-twin and twin-defect interactions to inform fundamental growth mechanisms in single crystal magnesium. (a) Evolution of twin area fraction for 1, 2, and 3 twin embryos. The inset shows the location of each twin for the three-embryo simulation. The area of the middle twin is measured using its length and width obtained from the interface profile at $\eta = 0.5$, as was done for Fig. 2; (b) Spatial distribution of the twin order parameter and shear stress in the parent and twin phases for the numerical setup shown in the inset of (a) at $t = 10$ and $t = 20$ ps; (c) Evolution of the shear stress along a horizontal line through the middle of the single crystal microstructure for different numbers of embryos. The numerical setup is subjected to 7% shear strain as was done in the other examples; (d) Study of twin-defect interactions by considering the time-evolved twin tip interface towards the boundary and the void. The related simulation dimensions are given in the inset, which also shows that symmetric boundary conditions were used (the symmetry line is shown by the dash red line). (For interpretation of the references to color in this figure, the reader is referred to the web version of this article.)

shear stress distribution, it is observed that the local shear stress reaches a minimum in the center of each twin. Outside the twins, the shear stress is lower at the bottom left and top right twins because of the constraining effect of the adjacent twins to the middle one. In the right insets, the deviatoric deformation in twin morphology at $t = 20$ ps is identified due to the interaction of the twins with each other and the disturbing of the stress field by them. The stress distribution in the vicinity of the twin-matrix interfaces at $t = 20$ ps is heterogeneous as a result of high stress concentrations in the matrix near the twin boundaries. It is also shown that the middle twin experiences a maximum shear stress resulting from the compressive forces generated by the other twins.

737
738
739
740
741
742
743
744
745
746
747
748
749
750
751
752
753
754
755
756
757
758
759
760
761
762
763
764
765
766
767
768
769
770
771
772
773
774
775
776
777
778
779
780
781
782

783 The local stress concentration is one main interaction of crack and twins where
784 some nucleation site appears in the interfaces inside and around the interface
785 [115].

786 Next, the change of shear stress along a horizontal line through a middle section
787 of the simulation area as a function of a 1, 2, or 3 embryo system is shown in
788 Fig. 4(c). It is observed that increasing the number of twins leads to decreasing
789 the shear stress values in the matrix phase, while the difference in shear stress
790 values for the later time instants are larger as a result of twin-twin interactions.
791 In the twinned regions at later times, the junctions of different embryos result
792 in a negative shear stress with steeper slopes as compared with earlier times.
793 In addition, it can be observed that the stress concentration in the matrix,
794 predominantly in the vicinity of the twin boundaries, increases only marginally
795 with increasing twin thickness (black lines in Fig. 4(c)). Finally, the interaction
796 of a twin and a defect is investigated in Fig. 4(d) by comparing the change in
797 the twin tip velocity towards the boundary and the void along the blue dashed
798 horizontal line. The numerical setup is also given in the inset, where symmetric
799 boundary conditions are used. The radius of 2 nm is chosen for the void. For
800 all times, the results indicate that the tip velocity is linearly decreasing in time
801 in a direction approaching the left boundary. For the void, the velocity at the
802 tip is constant until some point after which a sudden decrease in the velocity
803 occurs, resulting from the twin-defect interaction. In addition, the twin tip
804 velocity is larger toward the void because of the higher stress concentration
805 influenced by the void.

806

807 5 Conclusions

808

809 In this paper, the evolution of twinning in magnesium has been studied using a
810 validated and calibrated phase-field model to gain better insights into the time-
811 evolved twin morphology, the spatial distribution of the internal shear stress,
812 and the twin interactions. An accurate monolithic iterative procedure has been
813 implemented for solving the coupled balance and Ginzburg–Landau equations,
814 and the governing equations have been solved in the open-source high-level
815 computing platform, FEniCS. For engineering examples with FEniCS, we refer
816 to [116].

817 The results presented in this work confirmed the impact of the current
818 model by capturing the behavior of the leading deformation mechanism in
819 single crystal magnesium, twinning. By means of the proposed implementa-
820 tion, the state variables (i.e., the displacement and the twin order parameter)
821 have been computed monolithically for various scenarios in discrete time steps,
822 including small and large deformations with both isotropic and anisotropic sur-
823 face energies and elasticity. The data have been compared with a continuum
824 mechanics model [68] and molecular dynamics simulations [69]. The findings
825 are qualitatively consistent with both literature approaches.

826

827

828

A notable result emerging from the proposed model is the prediction of the critical strain and initial twin embryo size required for growth and propagation under the chosen numerical settings. This computational implementation is particularly useful because identifying such features experimentally is challenging given the length and time scales needed to reproduce these events [117]. Next, the interface velocities for the twin tips and twin boundaries have been explored in order to determine the kinetic coefficient using the phase-field model and compared with recent molecular dynamics simulation [69]. Studying velocity growths is important because they affect hardening, texture evolution, and ductility in the material [118]. To the authors' best knowledge, the present work pioneers the analysis of the interface mobility, showing different trends of twin evolution in the direction parallel and orthogonal to the twin habit plane.

The interface velocity is considered to be an important factor to determine the thermodynamic driving force for interface propagation, because knowing the interface velocity for any value of the driving force potentially leads to the determination of the kinetic coefficient for any range of materials [119]. The interface profile has been compared with the analytical solution of the stationary Ginzburg–Landau equation, and the obtained numerical interface width of 1.58 nm is close to the analytical value of 1.62 nm [70]. This information guides mesh selection and refinement when modeling twinning in this system [120]. In addition, the current phase-field modeling approach overcomes the challenges existing in molecular dynamic simulations for calculating the twin size, such as identifying the orientation of each atom in the twinned region [36], and is able to capture new behavior of twin growth for $t \leq 5$ ps, comparing well with previous molecular dynamics data [69]. The strong point of the current approach is to track multiple interfaces in order to measure twins' size with no additional efforts for samples larger or smaller than in atomistic simulations.

A further considerable implication of the proposed model is the possibility of investigating the local and global shear stress field inside the parent and twinned phases. Analysis of twin shear stress fields induced in these cases provides further evidence for the effect of twins' thickness and their mutual position on further twin growth and/or further twin nucleation [121–123]. Moreover, the importance of an appropriate strategy for partitioning the stress fields between the twinned and untwinned domains have been demonstrated in this paper. A final upshot of the current phase-field model has been to explore new understandings in twin-twin and twin-defect interactions. For the case where multiple twins grow in one grain, a common occurrence observed in experiments [124], it is highlighted that the stress concentration around the void may significantly increase the twin interface velocity, affecting subsequent expansion of the twins. Taken together, our study provides a framework for a new way to understand local deformation mechanisms in materials by analyzing the evolution and interaction of twins.

829
830
831
832
833
834
835
836
837
838
839
840
841
842
843
844
845
846
847
848
849
850
851
852
853
854
855
856
857
858
859
860
861
862
863
864
865
866
867
868
869
870
871
872
873
874

875 **6 Data Availability**

876 The authors declare that the main data supporting the findings of this
877 study are available within this article. Extra data are available from the
878 corresponding authors upon reasonable request.
879

880 **7 Code Availability**

881 The Python code, generated during the current study, is part of the FEniCS
882 project available at <http://www.fenicsproject.org/download>, and an example
883 for the computational implementation is available in [125] to be used under
884 the GNU Public license [126].
885

886 **8 Declaration of Competing Interests**

887 The authors declare no competing financial interests or personal relationships.
888

889 **9 CRediT Authorship Contributions Statement**

890 B.A developed the model, wrote the code, designed and performed all simu-
891 lations, analyzed results, and wrote the original draft. H.J analyzed results,
892 reviewed, and edited the paper. B.E.A developed the model and the code, allo-
893 cated the computational resources, reviewed and edited the paper. A.R helped
894 in computational aspects, reviewed and edited the paper. J.D.H supervised
895 the research, acquired funding, reviewed, and edited the paper. All authors
896 discussed the results.
897

900 **10 Acknowledgments**

901 The authors acknowledge support from Natural Sciences and Engineering
902 Research Council of Canada (NSERC) Discovery Grant 2016-04685 and
903 NSERC DNDPJ 531130-18, and partial support of the MIUR-PRIN project
904 XFAST-SIMS (no. 20173C478N).
905

906 **References**

- 907 [1] M. Chen, et al., Deformation twinning in nanocrystalline aluminum.
908 *Science* **300**(5623), 1275–1277 (2003). <https://doi.org/10.1126/science.1083727>. URL <https://science.sciencemag.org/content/300/5623/1275>.
909 <https://science.sciencemag.org/content/300/5623/1275.full.pdf>
910
- 911 [2] Q. Yu, et al., Strong crystal size effect on deformation twinning. *Nature*
912 **463**(7279), 335–338 (2010). <https://doi.org/10.1038/nature08692>. URL
913 <https://doi.org/10.1038/nature08692>
914

915
916
917
918
919
920

- [3] G. Chen, et al., Polysynthetic twinned tial single crystals for high-temperature applications. *Nature materials* **15**(8), 876–881 (2016). <https://doi.org/https://doi.org/10.1038/nmat4677> 921–924
- [4] J. Hirsch, T. Al-Samman, Superior light metals by texture engineering: Optimized aluminum and magnesium alloys for automotive applications. *Acta Materialia* **61**(3), 818–843 (2013). <https://doi.org/https://doi.org/10.1016/j.actamat.2012.10.044>. URL <https://www.sciencedirect.com/science/article/pii/S1359645412007914>. The Diamond Jubilee Issue 925–929
- [5] X.Z. Liao, et al., Deformation twinning in nanocrystalline copper at room temperature and low strain rate. *Applied Physics Letters* **84**(4), 592–594 (2004). <https://doi.org/10.1063/1.1644051>. URL <https://doi.org/10.1063/1.1644051>. <https://doi.org/10.1063/1.1644051> 930–934
- [6] X.Y. Zhang, et al., Growth of deformation twins in room-temperature rolled nanocrystalline nickel. *Applied Physics Letters* **94**(12), 121,907 (2009). <https://doi.org/10.1063/1.3104858>. URL <https://doi.org/10.1063/1.3104858> 935–939
- [7] R.J. McCabe, et al., Quantitative analysis of deformation twinning in zirconium. *International Journal of Plasticity* **25**(3), 454–472 (2009). <https://doi.org/https://doi.org/10.1016/j.ijplas.2008.03.010>. URL <https://www.sciencedirect.com/science/article/pii/S0749641908000569> 940–944
- [8] R.J. McCabe, et al., Deformation of wrought uranium: Experiments and modeling. *Acta Materialia* **58**(16), 5447–5459 (2010). <https://doi.org/https://doi.org/10.1016/j.actamat.2010.06.021>. URL <https://www.sciencedirect.com/science/article/pii/S1359645410003757> 945–949
- [9] T. Guo, et al., Analysing single twinning events in mg-6zn using nanoindentation. *Journal of Alloys and Compounds* **768**, 510–516 (2018). <https://doi.org/https://doi.org/10.1016/j.jallcom.2018.07.033>. URL <https://www.sciencedirect.com/science/article/pii/S09255838818325337> 950–954
- [10] Z. Wu, et al., Mechanistic origin and prediction of enhanced ductility in magnesium alloys. *Science* **359**(6374), 447 (2018). <https://doi.org/10.1126/science.aap8716>. URL <https://doi.org/10.1126/science.aap8716> 955–957
- [11] W.J. Joost, P.E. Krajewski, Towards magnesium alloys for high-volume automotive applications. *Scripta Materialia* **128**, 107–112 (2017). <https://doi.org/https://doi.org/10.1016/j.scriptamat.2016.07.035>. URL <https://www.sciencedirect.com/science/article/pii/S1359646216303621> 958–962
- [12] J. Wang, X. Wang, K. Yu, T.J. Rupert, S. Mahajan, E.J. Lavernia, J.M. Schoenung, I.J. Beyerlein, Manipulating deformation mechanisms with y alloying of mg. *Materials Science and Engineering: A* **817**, 141,373 963–966

- 967 (2021)
968
969 [13] A. Staroselsky, L. Anand, A constitutive model for hcp materials
970 deforming by slip and twinning: application to magnesium alloy az31b.
971 International journal of Plasticity **19**(10), 1843–1864 (2003)
972
973 [14] M. Lentz, et al., In situ x-ray diffraction and crystal plasticity modeling
974 of the deformation behavior of extruded mg–li–(al) alloys: An uncommon
975 tension–compression asymmetry. Acta Materialia **86**, 254–268 (2015).
976 <https://doi.org/https://doi.org/10.1016/j.actamat.2014.12.003>. URL
977 <https://www.sciencedirect.com/science/article/pii/S1359645414009112>
978
979 [15] L. Capolungo, et al., Slip-assisted twin growth in hexagonal close-
980 packed metals. Scripta Materialia **60**(1), 32–35 (2009). [https://doi.org/](https://doi.org/https://doi.org/10.1016/j.scriptamat.2008.08.044)
981 <https://doi.org/10.1016/j.scriptamat.2008.08.044>. URL [https://www.](https://www.sciencedirect.com/science/article/pii/S1359646208006374)
982 [sciencedirect.com/science/article/pii/S1359646208006374](https://www.sciencedirect.com/science/article/pii/S1359646208006374)
983
984 [16] J. Christian, S. Mahajan, Deformation twinning. Progress in Materials
985 Science **39**(1), 1–157 (1995). [https://doi.org/https://doi.org/10.1016/](https://doi.org/https://doi.org/10.1016/0079-6425(94)00007-7)
986 [0079-6425\(94\)00007-7](https://doi.org/10.1016/0079-6425(94)00007-7). URL [https://www.sciencedirect.com/science/](https://www.sciencedirect.com/science/article/pii/0079642594000077)
987 [article/pii/0079642594000077](https://www.sciencedirect.com/science/article/pii/0079642594000077)
988
989 [17] M. Arul Kumar, et al., Deformation twinning and grain partitioning in a
990 hexagonal close-packed magnesium alloy. Nature Communications **9**(1),
991 4761 (2018)
992
993 [18] B. Leu, M.A. Kumar, I.J. Beyerlein, The effects of free surfaces on
994 deformation twinning in hcp metals. Materialia **17**, 101,124 (2021)
995
996 [19] F. Yang, et al., Crack initiation mechanism of extruded az31 magne-
997 sium alloy in the very high cycle fatigue regime. Materials Science
998 and Engineering: A **491**(1), 131–136 (2008). <https://doi.org/https://doi.org/10.1016/j.msea.2008.02.003>. URL [https://www.sciencedirect.](https://www.sciencedirect.com/science/article/pii/S0921509308002074)
999 [com/science/article/pii/S0921509308002074](https://www.sciencedirect.com/science/article/pii/S0921509308002074)
1000
1001 [20] J. Tang, et al., Interactions between twin boundary and point defects in
1002 magnesium at low temperature. Journal of Materials Research pp. 1–12
1003 (2021). <https://doi.org/https://doi.org/10.1557/s43578-021-00120-w>
1004
1005 [21] H. Abdolvand, et al., Strong grain neighbour effects in polycrystals.
1006 Nature Communications **9**(1), 171 (2018). [https://doi.org/10.1038/](https://doi.org/10.1038/s41467-017-02213-9)
1007 [s41467-017-02213-9](https://doi.org/10.1038/s41467-017-02213-9). URL <https://doi.org/10.1038/s41467-017-02213-9>
1008
1009 [22] X. Zhao, et al., Direct observation and impact of co-segregated atoms in
1010 magnesium having multiple alloying elements. Nature Communications
1011 **10**(1), 3243 (2019). <https://doi.org/10.1038/s41467-019-10921-7>. URL
1012 <https://doi.org/10.1038/s41467-019-10921-7>

- [23] H. Fan, et al., Precipitation hardening effects on extension twinning in magnesium alloys. *International Journal of Plasticity* **106**, 186–202 (2018). <https://doi.org/https://doi.org/10.1016/j.ijplas.2018.03.008>. URL <https://www.sciencedirect.com/science/article/pii/S0749641917306721>
- [24] Y. Hu, et al., Embracing the chaos: Alloying adds stochasticity to twin embryo growth. *Phys. Rev. Lett.* **125**, 205,503 (2020). <https://doi.org/10.1103/PhysRevLett.125.205503>. URL <https://link.aps.org/doi/10.1103/PhysRevLett.125.205503>
- [25] J. Wang, et al., ($\bar{1}012$) twinning nucleation mechanisms in hexagonal-close-packed crystals. *Acta Materialia* **57**(18), 5521–5530 (2009). <https://doi.org/https://doi.org/10.1016/j.actamat.2009.07.047>. URL <https://www.sciencedirect.com/science/article/pii/S1359645409004832>
- [26] Y. Cao, et al., Twinning interactions induced amorphisation in ultrafine silicon grains. *Materials Science and Engineering: A* **658**, 321–325 (2016). <https://doi.org/https://doi.org/10.1016/j.msea.2016.02.014>. URL <https://www.sciencedirect.com/science/article/pii/S0921509316301307>
- [27] V. Kannan, et al., The mechanics of dynamic twinning in single crystal magnesium. *Journal of the Mechanics and Physics of Solids* **120**, 154–178 (2018). <https://doi.org/https://doi.org/10.1016/j.jmps.2018.03.010>. URL <https://www.sciencedirect.com/science/article/pii/S0022509617309201>. Special issue in honor of Ares J. Rosakis on the occasion of his 60th birthday
- [28] I.J. Beyerlein, et al., Statistical analyses of deformation twinning in magnesium. *Philosophical Magazine* **90**(16), 2161–2190 (2010). <https://doi.org/10.1080/14786431003630835>. URL <https://doi.org/10.1080/14786431003630835>
- [29] B. Li, E. Ma, Atomic shuffling dominated mechanism for deformation twinning in magnesium. *Phys. Rev. Lett.* **103**, 035,503 (2009). <https://doi.org/10.1103/PhysRevLett.103.035503>. URL <https://link.aps.org/doi/10.1103/PhysRevLett.103.035503>
- [30] J. Hirth, et al., Disconnections and other defects associated with twin interfaces. *Progress in Materials Science* **83**, 417–471 (2016). <https://doi.org/https://doi.org/10.1016/j.pmatsci.2016.07.003>. URL <https://www.sciencedirect.com/science/article/pii/S0079642516300329>
- [31] J. Zhang, et al., The dislocation-twin interaction and evolution of twin boundary in az31 mg alloy. *Acta Materialia* **133**, 208–216 (2017). <https://doi.org/https://doi.org/10.1016/j.actamat.2017.05.034>. URL <https://www.sciencedirect.com/science/article/pii/S1359645417300329>

- 1059 www.sciencedirect.com/science/article/pii/S1359645417304214
1060
- 1061 [32] Z. Wu, et al., Magnesium interatomic potential for simulating plasticity
1062 and fracture phenomena. *Modelling and Simulation in Materials Sci-*
1063 *ence and Engineering* **23**(1), 015,004 (2014). [https://doi.org/10.1088/](https://doi.org/10.1088/0965-0393/23/1/015004)
1064 [0965-0393/23/1/015004](https://doi.org/10.1088/0965-0393/23/1/015004). URL [https://doi.org/10.1088/](https://doi.org/10.1088/0965-0393/23/1/015004)
1065 [0965-0393/23/](https://doi.org/10.1088/0965-0393/23/1/015004)
1066 [1/015004](https://doi.org/10.1088/0965-0393/23/1/015004)
- 1067 [33] A.A. Benzerga, et al., Plastic flow anisotropy drives shear frac-
1068 ture. *Scientific Reports* **9**(1), 1425 (2019). [https://doi.org/10.1038/](https://doi.org/10.1038/s41598-018-38437-y)
1069 [s41598-018-38437-y](https://doi.org/10.1038/s41598-018-38437-y). URL [https://doi.org/10.1038/](https://doi.org/10.1038/s41598-018-38437-y)
1070 [s41598-018-38437-y](https://doi.org/10.1038/s41598-018-38437-y)
- 1071 [34] C.L. Kelchner, et al., Dislocation nucleation and defect structure during
1072 surface indentation. *Phys. Rev. B* **58**, 11,085–11,088 (1998). <https://doi.org/10.1103/PhysRevB.58.11085>. URL [https://link.aps.org/doi/](https://link.aps.org/doi/10.1103/PhysRevB.58.11085)
1073 [10.1103/PhysRevB.58.11085](https://link.aps.org/doi/10.1103/PhysRevB.58.11085)
- 1074
- 1075 [35] G.J. Ackland, A.P. Jones, Applications of local crystal structure mea-
1076 sures in experiment and simulation. *Phys. Rev. B* **73**, 054,104 (2006).
1077 <https://doi.org/10.1103/PhysRevB.73.054104>. URL [https://link.aps.](https://link.aps.org/doi/10.1103/PhysRevB.73.054104)
1078 [org/doi/10.1103/PhysRevB.73.054104](https://link.aps.org/doi/10.1103/PhysRevB.73.054104)
- 1079
- 1080 [36] G. Agarwal, A.M. Dongare, Deformation twinning in polycrys-
1081 talline mg microstructures at high strain rates at the atomic
1082 scales. *Scientific Reports* **9**(1), 3550 (2019). [https://doi.org/10.1038/](https://doi.org/10.1038/s41598-019-39958-w)
1083 [s41598-019-39958-w](https://doi.org/10.1038/s41598-019-39958-w). URL [https://doi.org/10.1038/](https://doi.org/10.1038/s41598-019-39958-w)
1084 [s41598-019-39958-w](https://doi.org/10.1038/s41598-019-39958-w)
- 1085 [37] R. Gluge, et al., A pseudoelastic model for mechanical twinning on the
1086 microscale. *ZAMM - Journal of Applied Mathematics and Mechanics /*
1087 *Zeitschrift fur Angewandte Mathematik und Mechanik* **90**(7-8), 565–594
1088 (2010). <https://doi.org/https://doi.org/10.1002/zamm.200900339>. URL
1089 <https://onlinelibrary.wiley.com/doi/abs/10.1002/zamm.200900339>.
1090 <https://onlinelibrary.wiley.com/doi/pdf/10.1002/zamm.200900339>
- 1091
- 1092 [38] J. Cheng, S. Ghosh, A crystal plasticity fe model for deformation with
1093 twin nucleation in magnesium alloys. *International Journal of Plasticity* **67**, 148–170 (2015). [https://doi.org/https://doi.org/10.1016/j.ijplas.](https://doi.org/https://doi.org/10.1016/j.ijplas.2014.10.005)
1094 [2014.10.005](https://doi.org/https://doi.org/10.1016/j.ijplas.2014.10.005). URL [https://www.sciencedirect.com/science/article/pii/](https://www.sciencedirect.com/science/article/pii/S0749641914001995)
1095 [S0749641914001995](https://www.sciencedirect.com/science/article/pii/S0749641914001995)
- 1096
- 1097 [39] V. Kolupaev, et al., Yield criteria of hexagonal symmetry in the π -plane.
1098 *Acta Mechanica* **224**(7), 1527–1540 (2013). <https://doi.org/https://doi.org/10.1007/s00707-013-0830-5>
1099 [https://doi.org/https://doi.org/10.1007/](https://doi.org/https://doi.org/10.1007/s00707-013-0830-5)
1100 [s00707-013-0830-5](https://doi.org/https://doi.org/10.1007/s00707-013-0830-5)
- 1101
- 1102 [40] C. Liu, et al., An integrated crystal plasticity–phase field model for spa-
1103 tially resolved twin nucleation, propagation, and growth in hexagonal
1104 materials. *International Journal of Plasticity* **106**, 203–227 (2018)

- [41] R. Kondo, et al., A phase-field model of twinning and detwinning coupled with dislocation-based crystal plasticity for hcp metals. *Computational Materials Science* **95**, 672–683 (2014). <https://doi.org/10.1016/j.commatsci.2014.08.034>. URL <https://www.sciencedirect.com/science/article/pii/S092702561400576X>
- [42] Y. Li, S. Hu, E. Barker, N. Overman, S. Whalen, S. Mathaudhu, Effect of grain structure and strain rate on dynamic recrystallization and deformation behavior: A phase field-crystal plasticity model. *Computational Materials Science* **180**, 109,707 (2020)
- [43] V.I. Levitas, Phase field approach for stress-and temperature-induced phase transformations that satisfies lattice instability conditions. part i. general theory. *International Journal of Plasticity* **106**, 164–185 (2018)
- [44] L.Q. Chen, Phase-field models for microstructure evolution. *Annual review of materials research* **32**(1), 113–140 (2002)
- [45] H. Hirshikesh, A. Pramod, H. Waisman, S. Natarajan, Adaptive phase field method using novel physics based refinement criteria. *Computer Methods in Applied Mechanics and Engineering* **383**, 113,874 (2021)
- [46] L.P. Yi, H. Waisman, Z.Z. Yang, X.G. Li, A consistent phase field model for hydraulic fracture propagation in poroelastic media. *Computer Methods in Applied Mechanics and Engineering* **372**, 113,396 (2020)
- [47] A.C. Hansen-Dörr, F. Dammaß, R. de Borst, M. Kästner, Phase-field modeling of crack branching and deflection in heterogeneous media. *Engineering Fracture Mechanics* **232**, 107,004 (2020)
- [48] C. Liu, P. Shanthraj, M. Diehl, F. Roters, S. Dong, J. Dong, W. Ding, D. Raabe, An integrated crystal plasticity–phase field model for spatially resolved twin nucleation, propagation, and growth in hexagonal materials. *International Journal of Plasticity* **106**, 203–227 (2018)
- [49] Z. Pi, Q. Fang, B. Liu, H. Feng, Y. Liu, Y. Liu, P. Wen, A phase field study focuses on the transverse propagation of deformation twinning for hexagonal-closed packed crystals. *International Journal of Plasticity* **76**, 130–146 (2016)
- [50] X. Hu, Y. Ji, T.W. Heo, L.Q. Chen, X. Cui, Phase-field model of deformation twin-grain boundary interactions in hexagonal systems. *Acta Materialia* **200**, 821–834 (2020)
- [51] X. Hu, Y. Ji, L. Chen, R.A. Lebensohn, L.Q. Chen, X. Cui, Spectral phase-field model of deformation twinning and plastic deformation. *International Journal of Plasticity* **143**, 103,019 (2021)

- 1151 [52] A. Ishii, Energetics of heterogeneous mg $\{101^{-} 2\}$ deformation twinning
1152 migration using an atomistically informed phase-field model. *Computa-*
1153 *tional Materials Science* **183**, 109,907 (2020)
1154
- 1155 [53] L.Q. Chen, J. Shen, Applications of semi-implicit fourier-spectral method
1156 to phase field equations. *Computer Physics Communications* **108**(2-3),
1157 147–158 (1998)
1158
- 1159 [54] V.A. Levin, V.I. Levitas, K.M. Zingerman, E.I. Freiman, Phase-field
1160 simulation of stress-induced martensitic phase transformations at large
1161 strains. *International Journal of Solids and Structures* **50**(19), 2914–2928
1162 (2013)
1163
- 1164 [55] M. Gong, J. Graham, V. Taupin, L. Capolungo, The effects of stress,
1165 temperature and facet structure on growth of $\{101^{-} 2\}$ twins in mg: A
1166 molecular dynamics and phase field study. *Acta Materialia* **208**, 116,603
1167 (2021)
1168
- 1169 [56] R. Ma, W. Sun, Phase field modeling of coupled crystal plasticity
1170 and deformation twinning in polycrystals with monolithic and splitting
1171 solvers. *International Journal for Numerical Methods in Engineering*
1172 **122**(4), 1167–1189 (2021)
1173
- 1174 [57] M.A. Kumar, A. Kanjarla, S. Niezgod, R. Lebensohn, C. Tomé, Numer-
1175 ical study of the stress state of a deformation twin in magnesium. *Acta*
1176 *Materialia* **84**, 349–358 (2015)
1177
- 1178 [58] K. Bhattacharya, et al., *Microstructure of martensite: why it forms and*
1179 *how it gives rise to the shape-memory effect*, vol. 2 (Oxford University
1180 Press, 2003)
1181
- 1182 [59] N. Grilli, A.C. Cocks, E. Tarleton, A phase field model for the growth
1183 and characteristic thickness of deformation-induced twins. *Journal of*
1184 *the Mechanics and Physics of Solids* **143**, 104,061 (2020)
1185
- 1186 [60] G. Liu, H. Mo, J. Wang, Y. Shen, Coupled crystal plasticity finite
1187 element-phase field model with kinetics-controlled twinning mechanism
1188 for hexagonal metals. *Acta Materialia* **202**, 399–416 (2021)
1189
- 1190 [61] J. Clayton, J. Knap, Phase field modeling and simulation of coupled
1191 fracture and twinning in single crystals and polycrystals. *Computer*
1192 *Methods in Applied Mechanics and Engineering* **312**, 447–467 (2016)
1193
- 1194 [62] R.Y. Zhang, et al., Parametric study of stress state development dur-
1195 1196 ing twinning using 3d finite element modeling. *Materials Science and*
Engineering: A **528**(6), 2725–2735 (2011). <https://doi.org/https://doi.org/10.1016/j.msea.2010.12.062>. URL <https://www.sciencedirect.com/>

- [science/article/pii/S0921509310014693](https://doi.org/10.1016/j.actamat.2016.06.042) 1197
1198
- [63] M. Arul Kumar, et al., Effect of local stress fields on twin characteristics in hcp metals. *Acta Materialia* **116**, 143–154 (2016). [https://doi.org/https://doi.org/10.1016/j.actamat.2016.06.042](https://doi.org/10.1016/j.actamat.2016.06.042). URL <https://www.sciencedirect.com/science/article/pii/S1359645416304621> 1199
1200
1201
1202
1203
- [64] C. Schreiber, C. Kuhn, R. Müller, T. Zohdi, A phase field modeling approach of cyclic fatigue crack growth. *International Journal of Fracture* **225**(1), 89–100 (2020) 1204
1205
1206
1207
- [65] A. Schlüter, A. Willenbücher, C. Kuhn, R. Müller, Phase field approximation of dynamic brittle fracture. *Computational Mechanics* **54**(5), 1141–1161 (2014) 1208
1209
1210
1211
- [66] A.C. Hansen-Dörr, R. de Borst, P. Hennig, M. Kästner, Phase-field modelling of interface failure in brittle materials. *Computer Methods in Applied Mechanics and Engineering* **346**, 25–42 (2019) 1212
1213
1214
1215
- [67] P. Rosakis, H. Tsai, Dynamic twinning processes in crystals. *International journal of solids and structures* **32**(17-18), 2711–2723 (1995) 1216
1217
- [68] J. Clayton, J. Knap, A phase field model of deformation twinning: Nonlinear theory and numerical simulations. *Physica D: Nonlinear Phenomena* **240**(9), 841–858 (2011). [https://doi.org/https://doi.org/10.1016/j.physd.2010.12.012](https://doi.org/10.1016/j.physd.2010.12.012). URL <https://www.sciencedirect.com/science/article/pii/S0167278910003623> 1218
1219
1220
1221
1222
1223
- [69] Y. Hu, et al., Disconnection-mediated twin embryo growth in mg. *Acta Materialia* **194**, 437–451 (2020). [https://doi.org/https://doi.org/10.1016/j.actamat.2020.04.010](https://doi.org/10.1016/j.actamat.2020.04.010). URL <https://www.sciencedirect.com/science/article/pii/S1359645420302676> 1224
1225
1226
1227
1228
- [70] A.V. Lyulin, N.K. Balabaev, M.A. Mazo, M. Michels, Molecular dynamics simulation of uniaxial deformation of glassy amorphous atactic polystyrene. *Macromolecules* **37**(23), 8785–8793 (2004) 1229
1230
1231
1232
- [71] H. Park, J. Choi, B. Kim, S. Yang, H. Shin, M. Cho, Toward the constitutive modeling of epoxy matrix: Temperature-accelerated quasi-static molecular simulations consistent with the experimental test. *Composites Part B: Engineering* **142**, 131–141 (2018) 1233
1234
1235
1236
1237
- [72] J.R. Rice, Inelastic constitutive relations for solids: an internal-variable theory and its application to metal plasticity. *Journal of the Mechanics and Physics of Solids* **19**(6), 433–455 (1971) 1238
1239
1240
1241
1242

- 1243 [73] H. Yagyu, Coarse-grained molecular dynamics simulation of the effects of
1244 strain rate on tensile stress of cross-linked rubber. *Soft Materials* **13**(4),
1245 263–270 (2015)
1246
- 1247 [74] E.V. Struleva, P.S. Komarov, S.I. Ashitkov, Dynamic strength of tita-
1248 nium melt at extremely high extension rates. *High Temperature* **57**(6),
1249 948–950 (2019)
1250
- 1251 [75] G.H. Farrahi, M. Javanbakht, H. Jafarzadeh, On the phase field modeling
1252 of crack growth and analytical treatment on the parameters. *Continuum*
1253 *Mechanics and Thermodynamics* **32**(3), 589–606 (2020)
1254
- 1255 [76] L. Farbaniec, et al., Spall response and failure mechanisms associated
1256 with a hot-extruded amx602 mg alloy. *Materials Science and Engineer-*
1257 *ing: A* **707**, 725–731 (2017). [https://doi.org/https://doi.org/10.1016/j.](https://doi.org/https://doi.org/10.1016/j.msea.2017.09.105)
1258 [msea.2017.09.105](https://doi.org/https://doi.org/10.1016/j.msea.2017.09.105). URL [https://www.sciencedirect.com/science/article/](https://www.sciencedirect.com/science/article/pii/S0921509317312753)
1259 [pii/S0921509317312753](https://www.sciencedirect.com/science/article/pii/S0921509317312753)
- 1260 [77] R.D. James, Finite deformation by mechanical twinning. *Archive for*
1261 *Rational Mechanics and Analysis* **77**(2), 143–176 (1981)
1262
- 1263 [78] V.I. Levitas, D.L. Preston, Three-dimensional landau theory for
1264 multivariant stress-induced martensitic phase transformations. i.
1265 austenite \leftrightarrow martensite. *Phys. Rev. B* **66**, 134,206 (2002). [https://](https://doi.org/10.1103/PhysRevB.66.134206)
1266 doi.org/10.1103/PhysRevB.66.134206. URL [https://link.aps.org/doi/](https://link.aps.org/doi/10.1103/PhysRevB.66.134206)
1267 [10.1103/PhysRevB.66.134206](https://link.aps.org/doi/10.1103/PhysRevB.66.134206)
1268
- 1269 [79] V.I. Levitas, D.L. Preston, Thermomechanical lattice instability and
1270 phase field theory of martensitic phase transformations, twinning and
1271 dislocations at large strains. *Physics Letters A* **343**(1), 32–39 (2005).
1272 <https://doi.org/https://doi.org/10.1016/j.physleta.2005.05.034>. URL
1273 <https://www.sciencedirect.com/science/article/pii/S0375960105007644>
1274
- 1275 [80] R. Hill, The elastic behaviour of a crystalline aggregate. *Proceedings of*
1276 *the Physical Society. Section A* **65**(5), 349 (1952)
1277
- 1278 [81] J. Clayton, A continuum description of nonlinear elasticity, slip and
1279 twinning, with application to sapphire. *Proceedings of the Royal Soci-*
1280 *ety A: Mathematical, Physical and Engineering Sciences* **465**(2101),
1281 307–334 (2009). <https://doi.org/10.1098/rspa.2008.0281>. URL
1282 <https://royalsocietypublishing.org/doi/abs/10.1098/rspa.2008.0281>.
1283 <https://royalsocietypublishing.org/doi/pdf/10.1098/rspa.2008.0281>
1284
- 1285 [82] V.I. Levitas, et al., Displacive phase transitions at large strains: Phase-
1286 field theory and simulations. *Phys. Rev. Lett.* **103**, 025,702 (2009). [https://](https://doi.org/10.1103/PhysRevLett.103.025702)
1287 doi.org/10.1103/PhysRevLett.103.025702. URL [https://link.aps.org/](https://link.aps.org/doi/10.1103/PhysRevLett.103.025702)
1288 [doi/10.1103/PhysRevLett.103.025702](https://link.aps.org/doi/10.1103/PhysRevLett.103.025702)

- [83] V.I. Levitas, Phase field approach to martensitic phase transformations with large strains and interface stresses. *Journal of the Mechanics and Physics of Solids* **70**, 154–189 (2014). <https://doi.org/https://doi.org/10.1016/j.jmps.2014.05.013>. URL <https://www.sciencedirect.com/science/article/pii/S0022509614001045>
- [84] T.I. Zohdi, *Finite element primer for beginners* (Springer)
- [85] J. Chung, G. Hulbert, A time integration algorithm for structural dynamics with improved numerical dissipation: the generalized- α method (1993)
- [86] A. Logg, G.N. Wells, Dolfin: Automated finite element computing. *ACM Trans. Math. Softw.* **37**(2) (2010). <https://doi.org/10.1145/1731022.1731030>. URL <https://doi.org/10.1145/1731022.1731030>
- [87] K.B. Ølgaard, et al., Automated code generation for discontinuous galerkin methods. *SIAM Journal on Scientific Computing* **31**(2), 849–864 (2009). <https://doi.org/10.1137/070710032>. URL <https://doi.org/10.1137/070710032>. <https://doi.org/10.1137/070710032>
- [88] S. Balay, S. Abhyankar, M.F. Adams, J. Brown, P. Brune, K. Buschelman, L. Dalcin, A. Dener, V. Eijkhout, W.D. Gropp, D. Karpeyev, D. Kaushik, M.G. Knepley, D.A. May, L.C. McInnes, R.T. Mills, T. Munson, K. Rupp, P. Sanan, B.F. Smith, S. Zampini, H. Zhang, H. Zhang, PETSc users manual. Tech. Rep. ANL-95/11 - Revision 3.15, Argonne National Laboratory (2021). <https://doi.org/https://www.mcs.anl.gov/petsc>
- [89] L.J. Slutsky, C.W. Garland, Elastic constants of magnesium from 4.2°K to 300°K. *Phys. Rev.* **107**, 972–976 (1957). <https://doi.org/10.1103/PhysRev.107.972>. URL <https://link.aps.org/doi/10.1103/PhysRev.107.972>
- [90] J. Lee, M. Yoo, Elastic strain energy of deformation twinning in tetragonal crystals. *Metallurgical Transactions A* **21**(9), 2521–2530 (1990)
- [91] A. Staroselsky, L. Anand, A constitutive model for hcp materials deforming by slip and twinning: application to magnesium alloy az31b. *International Journal of Plasticity* **19**(10), 1843–1864 (2003)
- [92] S. Kavousi, B.R. Novak, M.A. Zaeem, D. Moldovan, Combined molecular dynamics and phase field simulation investigations of crystal-melt interfacial properties and dendritic solidification of highly undercooled titanium. *Computational Materials Science* **163**, 218–229 (2019)

- 1335 [93] A.M. Kosevich, V.S. Bouko, Dislocation theory of the elastic twinning
1336 of crystals. *Soviet Physics Uspekhi* **14**(3), 286–316 (1971)
1337
- 1338 [94] J. Wang, N. Li, O. Anderoglu, X. Zhang, A. Misra, J. Huang, J. Hirsh,
1339 Detwinning mechanisms for growth twins in face-centered cubic metals.
1340 *Acta Materialia* **58**(6), 2262–2270 (2010). <https://doi.org/https://doi.org/10.1016/j.actamat.2009.12.013>. URL <https://www.sciencedirect.com/science/article/pii/S1359645409008556>
1341
1342
- 1343 [95] S. Lee, J. Im, Y. Yoo, E. Bitzek, D. Kiener, G. Richter, B. Kim,
1344 S.H. Oh, Reversible cyclic deformation mechanism of gold nanowires by
1345 twinning–detwinning transition evidenced from in situ tem. *Nature com-*
1346 *munications* **5**(1), 1–10 (2014). <https://doi.org/10.1038/ncomms4033>
1347
- 1348 [96] K. Máthis, et al., On the dynamics of twinning in magnesium micropil-
1349 lars. *Materials & Design* **203**, 109,563 (2021). <https://doi.org/https://doi.org/10.1016/j.matdes.2021.109563>. URL <https://www.sciencedirect.com/science/article/pii/S0264127521001167>
1350
1351
1352
- 1353 [97] B. Morrow, et al., Toward understanding twin–twin interactions in
1354 hcp metals: Utilizing multiscale techniques to characterize deformation
1355 mechanisms in magnesium. *Materials Science and Engineering: A*
1356 **613**, 365–371 (2014). <https://doi.org/https://doi.org/10.1016/j.msea.2014.06.062>. URL <https://www.sciencedirect.com/science/article/pii/S0921509314007795>
1357
1358
1359
- 1360 [98] S. Bergmann, K. Albe, E. Flegel, D. Barragan-Yani, B. Wagner,
1361 Anisotropic solid–liquid interface kinetics in silicon: an atomistically
1362 informed phase-field model. *Modelling and Simulation in Materials*
1363 *Science and Engineering* **25**(6), 065,015 (2017)
1364
- 1365 [99] B. Clausen, et al., Reorientation and stress relaxation due to twinning:
1366 Modeling and experimental characterization for mg. *Acta Materialia*
1367 **56**(11), 2456–2468 (2008)
1368
- 1369 [100] C. Mareau, M.R. Daymond, Micromechanical modelling of twinning in
1370 polycrystalline materials: Application to magnesium. *International Jour-*
1371 *nal of Plasticity* **85**, 156–171 (2016). <https://doi.org/https://doi.org/10.1016/j.ijplas.2016.07.007>. URL <https://www.sciencedirect.com/science/article/pii/S0749641916301140>
1372
1373
- 1374 [101] A. Hürkamp, et al., Combining simulation and machine learning as
1375 digital twin for the manufacturing of overmolded thermoplastic compos-
1376 ites. *Journal of Manufacturing and Materials Processing* **4**(3) (2020).
1377 <https://doi.org/10.3390/jmmp4030092>. URL <https://www.mdpi.com/2504-4494/4/3/92>
1378
1379
1380

- [102] F. dell’Isola, D.J. Steigmann, *Discrete and Continuum Models for Complex Metamaterials* (Cambridge University Press, 2020) 1381
1382
1383
- [103] I. Giorgio, A. Ciallella, D. Scerrato, A study about the impact of the topological arrangement of fibers on fiber-reinforced composites: some guidelines aiming at the development of new ultra-stiff and ultra-soft metamaterials. *International Journal of Solids and Structures* **203**, 73–83 (2020) 1384
1385
1386
1387
1388
1389
- [104] E. Barchiesi, M. Spagnuolo, L. Placidi, Mechanical metamaterials: a state of the art. *Mathematics and Mechanics of Solids* **24**(1), 212–234 (2019) 1390
1391
1392
- [105] J.M. Hu, et al., Understanding and designing magnetoelectric heterostructures guided by computation: progresses, remaining questions, and perspectives. *npj Computational Materials* **3**(1), 1–21 (2017). <https://doi.org/https://doi.org/10.1038/s41524-017-0020-4> 1393
1394
1395
1396
- [106] F. dell’Isola, C. Woźniak, On phase transition layers in certain micro-damaged two-phase solids. *International Journal of Fracture* **83**(2), 175–189 (1997) 1397
1398
1399
1400
- [107] F. Aldakheel, A microscale model for concrete failure in poro-elasto-plastic media. *Theoretical and Applied Fracture Mechanics* **107**, 102,517 (2020) 1401
1402
1403
1404
- [108] A. Madeo, A.D. Corte, I. Giorgio, D. Scerrato, Modeling and designing micro-and nano-structured metamaterials: towards the application of exotic behaviors. *Mathematics and Mechanics of Solids* **22**(4), 873–884 (2017) 1405
1406
1407
1408
1409
- [109] I. Temizer, P. Wriggers, A micromechanically motivated higher-order continuum formulation of linear thermal conduction. *ZAMM-Journal of Applied Mathematics and Mechanics/Zeitschrift für Angewandte Mathematik und Mechanik* **90**(10-11), 768–782 (2010) 1410
1411
1412
1413
1414
- [110] M. Cottura, Y. Le Bouar, A. Finel, B. Appolaire, K. Ammar, S. Forest, A phase field model incorporating strain gradient viscoplasticity: application to rafting in ni-base superalloys. *Journal of the Mechanics and Physics of Solids* **60**(7), 1243–1256 (2012) 1415
1416
1417
1418
1419
- [111] F. Aldakheel, *Mechanics of nonlocal dissipative solids: gradient plasticity and phase field modeling of ductile fracture* (Stuttgart: Institut für Mechanik (Bauwesen), Lehrstuhl I, Universität Stuttgart, 2016) 1420
1421
1422
- [112] L. Placidi, E. Barchiesi, A. Misra, A strain gradient variational approach to damage: a comparison with damage gradient models and numerical results. *Mathematics and Mechanics of Complex Systems* **6**(2), 77–100 1423
1424
1425
1426

- 1427 (2018)
1428
- 1429 [113] F. Dammaß, M. Ambati, M. Kästner, A unified phase-field model of
1430 fracture in viscoelastic materials. *Continuum Mechanics and Thermo-*
1431 *dynamics* pp. 1–23 (2021)
1432
- 1433 [114] B.E. Abali, A. Klunker, E. Barchiesi, L. Placidi, A novel phase-field
1434 approach to brittle damage mechanics of gradient metamaterials combin-
1435 ing action formalism and history variable. *ZAMM-Journal of Applied*
1436 *Mathematics and Mechanics/Zeitschrift für Angewandte Mathematik*
1437 *und Mechanik* p. e202000289 (2021)
1438
- 1439 [115] S. Forest, R. Parisot, Material crystal plasticity and deformation twin-
1440 ning. *Rendiconti del Seminario Matematico dell’Universita e del*
1441 *Politecnico di Torino* **58**, 99–111 (2000)
1442
- 1443 [116] Q. Sun, et al., Investigation of twin–twin interaction in
1444 deformed magnesium alloy. *Philosophical Magazine* **98**(9),
1445 741–751 (2018). [https://doi.org/10.1080/14786435.2017.](https://doi.org/10.1080/14786435.2017.1417648)
1446 [1417648](https://doi.org/10.1080/14786435.2017.1417648). URL <https://doi.org/10.1080/14786435.2017.1417648>.
1447 <https://doi.org/10.1080/14786435.2017.1417648>
1448
- 1449 [117] G.D. Sim, et al., Anomalous hardening in magnesium driven by a
1450 size-dependent transition in deformation modes. *Acta Materialia*
1451 **144**, 11–20 (2018). [https://doi.org/https://doi.org/10.1016/j.actamat.](https://doi.org/https://doi.org/10.1016/j.actamat.2017.10.033)
1452 [2017.10.033](https://doi.org/https://doi.org/10.1016/j.actamat.2017.10.033). URL [https://www.sciencedirect.com/science/article/pii/](https://www.sciencedirect.com/science/article/pii/S1359645417308911)
1453 [S1359645417308911](https://www.sciencedirect.com/science/article/pii/S1359645417308911)
1454
- 1455 [118] S.R. Yeratapally, et al., Microstructure based fatigue life prediction
1456 framework for polycrystalline nickel-base superalloys with emphasis on
1457 the role played by twin boundaries in crack initiation. *Acta Mate-*
1458 *rialia* **107**, 152–167 (2016). [https://doi.org/https://doi.org/10.1016/](https://doi.org/https://doi.org/10.1016/j.actamat.2016.01.038)
1459 [j.actamat.2016.01.038](https://doi.org/https://doi.org/10.1016/j.actamat.2016.01.038). URL [https://www.sciencedirect.com/science/](https://www.sciencedirect.com/science/article/pii/S1359645416300374)
1460 [article/pii/S1359645416300374](https://www.sciencedirect.com/science/article/pii/S1359645416300374)
1461
- 1462 [119] M. Bönisch, et al., Hardening by slip-twin and twin-twin interactions
1463 in femnicrocr. *Acta Materialia* **153**, 391–403 (2018). [https://doi.](https://doi.org/https://doi.org/10.1016/j.actamat.2018.04.054)
1464 [org/https://doi.org/10.1016/j.actamat.2018.04.054](https://doi.org/https://doi.org/10.1016/j.actamat.2018.04.054). URL [https://www.](https://www.sciencedirect.com/science/article/pii/S1359645418303318)
1465 [sciencedirect.com/science/article/pii/S1359645418303318](https://www.sciencedirect.com/science/article/pii/S1359645418303318)
1466
- 1467 [120] J. Cheng, S. Ghosh, Crystal plasticity finite element modeling of discrete
1468 twin evolution in polycrystalline magnesium. *Journal of the Mechanics*
1469 *and Physics of Solids* **99**, 512–538 (2017). [https://doi.org/https://doi.](https://doi.org/https://doi.org/10.1016/j.jmps.2016.12.008)
1470 [org/10.1016/j.jmps.2016.12.008](https://doi.org/https://doi.org/10.1016/j.jmps.2016.12.008). URL [https://www.sciencedirect.com/](https://www.sciencedirect.com/science/article/pii/S0022509616304641)
1471 [science/article/pii/S0022509616304641](https://www.sciencedirect.com/science/article/pii/S0022509616304641)
1472

- [121] H. Jafarzadeh, et al., Phase field approach for nanoscale interactions between crack propagation and phase transformation. *Nanoscale* **11**, 22,243–22,247 (2019). <https://doi.org/10.1039/C9NR05960A>. URL <http://dx.doi.org/10.1039/C9NR05960A>
- [122] B.E. Abali, *Computational Reality, Advanced Structured Materials*, vol. 55 (Springer Nature, Singapore, 2017)
- [123] Y. Liu, et al., Experimentally quantifying critical stresses associated with basal slip and twinning in magnesium using micropillars. *Acta Materialia* **135**, 411–421 (2017). <https://doi.org/https://doi.org/10.1016/j.actamat.2017.06.008>. URL <https://www.sciencedirect.com/science/article/pii/S1359645417304792>
- [124] M. Gong, et al., Atomistic simulations of interaction between basal α_2 dislocations and three-dimensional twins in magnesium. *Acta Materialia* **155**, 187–198 (2018). <https://doi.org/https://doi.org/10.1016/j.actamat.2018.05.066>. URL <https://www.sciencedirect.com/science/article/pii/S1359645418304579>
- [125] V.I. Levitas, Phase-field theory for martensitic phase transformations at large strains. *International Journal of Plasticity* **49**, 85–118 (2013). <https://doi.org/https://doi.org/10.1016/j.ijplas.2013.03.002>. URL <https://www.sciencedirect.com/science/article/pii/S0749641913000727>
- [126] K. Momeni, V.I. Levitas, A phase-field approach to solid–solid phase transformations via intermediate interfacial phases under stress tensor. *International Journal of Solids and Structures* **71**, 39–56 (2015). <https://doi.org/https://doi.org/10.1016/j.ijsolstr.2015.05.027>. URL <https://www.sciencedirect.com/science/article/pii/S0020768315002450>
- [127] J. Robson, The effect of internal stresses due to precipitates on twin growth in magnesium. *Acta Materialia* **121**, 277–287 (2016). <https://doi.org/https://doi.org/10.1016/j.actamat.2016.09.022>. URL <https://www.sciencedirect.com/science/article/pii/S1359645416307108>
- [128] D. Jang, et al., Deformation mechanisms in nanotwinned metal nanopillars. *Nature nanotechnology* **7**(9), 594 (2012). <https://doi.org/https://doi.org/10.1038/nnano.2012.116>
- [129] W. Hutchinson, M. Barnett, Effective values of critical resolved shear stress for slip in polycrystalline magnesium and other hcp metals. *Scripta Materialia* **63**(7), 737–740 (2010). <https://doi.org/https://doi.org/10.1016/j.scriptamat.2010.05.047>. URL <https://www.sciencedirect.com/science/article/pii/S1359646210003726>. Viewpoint set no. 47 Magnesium Alloy Science and Technology

- 1519 [130] J. Jung, et al., Continuum understanding of twin formation near grain
1520 boundaries of fcc metals with low stacking fault energy. *npj Computa-*
1521 *tional Materials* **3**(1), 1–9 (2017). [https://doi.org/https://doi.org/10.](https://doi.org/https://doi.org/10.1038/s41524-017-0023-1)
1522 [1038/s41524-017-0023-1](https://doi.org/https://doi.org/10.1038/s41524-017-0023-1)
1523
- 1524 [131] B.E. Abali. Supply code for computations (2020). [https://doi.org/http:](https://doi.org/http://bilenemek.abali.org/)
1525 [//bilenemek.abali.org/](https://doi.org/http://bilenemek.abali.org/)
1526
- 1527 [132] GNU Public. Gnu general public license (2007). [https://doi.org/http:](https://doi.org/http://www.gnu.org/copyleft/gpl.html)
1528 [//www.gnu.org/copyleft/gpl.html](https://doi.org/http://www.gnu.org/copyleft/gpl.html)
1529
1530
1531
1532
1533
1534
1535
1536
1537
1538
1539
1540
1541
1542
1543
1544
1545
1546
1547
1548
1549
1550
1551
1552
1553
1554
1555
1556
1557
1558
1559
1560
1561
1562
1563
1564

For Peer Review